

Design and Evaluation of GNSS/INS Tightly-Coupled Navigation Software for Land Vehicles

Zhi Chao. Wen¹, You. Li^{2,3}, Xue Li. Guo², Xuan Xuan. Zhang⁴

1 China University of Geosciences, Beijing, China - 1046407953@qq.com.

2 State Key Laboratory of Information Engineering in Surveying, Mapping and Remote Sensing, Wuhan University, Wuhan, China - liyou@whu.edu.cn, China - guoxueli@whu.edu.cn.

3 Hubei LuoJia Laboratory, Wuhan, China.

4 Chinese Academy of surveying and mapping, Beijing, China - 779865060@qq.com.

Commission III, WG III/1

KEY WORDS: GNSS/INS, Tightly-Coupled Navigation, Land Vehicles, PPP.

ABSTRACT

Due to the development of society, the city center is full of high-rise buildings and the traffic becomes increasingly convenient; accordingly, there is a high demand for high-precision navigation in such areas. This paper studied the GNSS/Inertial Navigation System (INS) integrated navigation algorithm and developed software that can process GNSS data and IMU data. To verify the positioning performance of the algorithm, we collect the data of onboard GNSS and IMU in an urban environment and compare the results of GNSS positioning and GNSS/INS tightly-coupled navigation. The horizontal and 3D positioning accuracy of GNSS/INS tightly coupling is better than 0.8 m and 1.2 m, respectively. Compared to GNSS, the 3D and horizontal position precision of GNSS/INS tightly coupling improved by 17.4 % and 54.9 %, respectively. It proves that the GNSS/INS tightly-coupled navigation can provide higher-precision and more robust positioning results.

1. INTRODUCTION

With the development of society, the global navigation satellite system (GNSS) has been widely used in various fields, such as meteorology, vehicle navigation, precision agriculture, and disaster monitoring (Aykut, 2018; Erol, 2020; Guo et al., 2018; Guo et al., 2019). GNSS provides users high-precision positioning, velocity, and timing service day and night. In recent years, GNSS has been continuously developed and improved. Precision single-point positioning (PPP) is a mainstream high-precision positioning technology. For PPP, some scholars proved that the PPP algorithm can provide high-precision positioning results, and using multi-frequency and multi-mode GNSS data can improve positioning accuracy and convergence time (Li et al., 2020). However, in the complex urban environment, fewer observable satellites and serious multipath effects will reduce the positioning precision. Therefore, a more reliable navigation solution is required (Li et al., 2021). To meet this requirement, scholars focus on navigation based on the integration of GNSS and multiple sensors, such as IMU, RGB camera, lidar, odometer, and magnetometer (Zhao et al., 2020).

GNSS/INS coupled navigation is one of the research hotspots at present (Chen et al., 2021; Jiang et al., 2021; Zhang et al., 2020). Inertial navigation system (INS) can provide high-precision position and velocity information in a short time and is not affected by the environment, but the positioning error will accumulate rapidly over time and rely on high-precision initial position and velocity information (Li et al., 2014). The combination of GNSS and INS can make up for various defects. GNSS provides INS high-precision initial position and speed information and avoids the accumulation of positioning errors (Abdolkarimi, Mosavi, 2020). INS can also obtain high-precision navigation results when the GNSS satellite signal is weak or even out of the lock in a short time. Therefore, even in the complex urban environment, GNSS/INS coupled navigation can still get high-precision, stable, and reliable navigation results (Falco et al., 2017; Gu et al., 2021; Shi et al., 2021).

This paper studied the algorithm based on GNSS/INS coupled navigation and developed a software that can process GNSS data and IMU data based on MATLAB. First, we will briefly introduce the software. Then, a brief description of the theory of GNSS/INS tightly-coupled navigation. Afterward, the experimental results are presented and analyzed, which validate and assess the performance of our software. Finally, we summarize the main conclusions in the last section.

2. MATHEMATICAL MODEL

2.1 GNSS model

GNSS basic observation equation:

$$\begin{cases} P_{r,f}^{s,T} = \rho + c(t_r - t^{s,T}) + Ion_{r,f}^{s,T} + Trop \\ \quad + (d_{r,f}^T - d_f^{s,T}) + \epsilon_{r,f}^{s,T} \\ L_{r,f}^{s,T} = \rho + c(t_r - t^{s,T}) - Ion_{r,f}^{s,T} + Trop \\ \quad + \lambda_f^{s,T} (N_{r,f}^{s,T} + b_{r,f}^T - b_f^{s,T}) + \xi_{r,f}^{s,T} \end{cases} \quad (1)$$

where Superscript and subscript s, r, f, T represent the satellite, receiver, carrier frequency band, and satellite system, respectively. P and L are pseudo range and carrier observations, respectively; ρ is the distance from the satellite to the receiver; t_r and $t^{s,T}$ are receiver clock error and satellite clock error respectively; Ion and $Trop$ are Ionospheric delay and tropospheric delay; $d_{r,f}^T$ and $d_f^{s,T}$ are code bias on receiver and satellite respectively; $b_{r,f}^T$ and $b_f^{s,T}$ are phase bias on receiver and satellite respectively; $\lambda_f^{s,T}$ are wavelength; $N_{r,f}^{s,T}$ are ambiguity; $\epsilon_{r,f}^{s,T}$ and $\xi_{r,f}^{s,T}$ are the sum of observation noise and multipath error on pseudo range and carrier respectively;

Antenna phase center offset (PCO) and phase center variety (PCV) of receiver and satellite, relativistic effect, sagnac effect, phase windup, ocean tide error need to be corrected according to the priori model. Ionospheric delay parameters are constrained using global ionospheric model (GIM) products. Linearize (1) can obtain

$$\left\{ \begin{array}{l} \Delta P_{r,f}^{s,T} = \mu_{r,f}^{s,T} \cdot x + \hat{c}_r + Ion_{r,f}^{s,T} + Trop \\ \quad + \beta^T (DCB_r^T + DCB^{s,T}) + \varepsilon_{r,f}^{s,T} \\ \Delta L_{r,f}^{s,T} = \mu_{r,f}^{s,T} \cdot x + \hat{c}_r - Ion_{r,f}^{s,T} + Trop \\ - \beta^T (DCB_r^T + DCB^{s,T}) + \lambda_f^{s,T} \bar{N}_{r,f}^{s,T} + \xi_{r,f}^{s,T} \\ Ion_{GIM}^{s,T} = Ion_{r,f}^{s,T} \end{array} \right. \quad (2)$$

where ΔP and ΔL are pseudo range and carrier observations minus the calculated values, respectively. $\mu_r^{s,T}$ and x are the direction vector from the receiver to the satellite and the position vector of the receiver. DCB_r^T and $DCB^{s,T}$ differential code bias of receiver and satellite. Coefficient $\beta^T = -\frac{(f_2^{s,T})^2}{(f_1^{s,T})^2 - (f_2^{s,T})^2}$.

In equation 2, the value of satellite difference code bias (DCB) is very stable within one month and can be corrected directly with DCB products. However, DCB products only have the receiver DCB of some IGS stations, so the receiver DCB is solved as an unknown number. The corresponding observation model matrix is as

$$\begin{cases} Z = H_{GNSS}X_{GNSS} + \varepsilon \\ Z = [P_1 \quad P_2 \quad L_1 \quad L_2 \quad I]^T \\ X_{GNSS} = [x \quad \hat{ct}_r \quad DCB \quad Ion \quad Trop \quad N]^T \\ H_{GNSS} = \begin{bmatrix} H_x & H_{\hat{ct}_r} & H_{DCB} & H_{Ion} & H_{Trop} & H_N \\ 0 & 0 & 0 & I & 0 & 0 \end{bmatrix} \end{cases} \quad (3)$$

where \mathbf{z} , H_{GNSS} , X_{GNSS} are observation vector, design matrix, and state vector. Ion is the ionospheric delay of all satellites observed for this epoch; $N = [N_1 \ N_2]$ are the ambiguity of all satellite carrier observations L1 and L2.

2.2 INS model

INS calculates the state of the carrier in the next epoch according to the initial state (position, velocity, and attitude) and the observed values (velocity increment and angular velocity increment or specific force and acceleration). This process is also called mechanical arrangement. There are several error models of INS, the most classic are psi angle model and phi angle model. In this paper, psi angle model is used to calculate the error equation of velocity, position, and attitude in the computer coordinate system (c-frame):

$$\left. \begin{aligned} \delta \dot{v}^c &= f^c \times \psi + C_b^p \delta f^b - (\omega_{ie}^c + \omega_{ic}^c) \times \delta v^c + \delta g^c \\ \delta \dot{p}^c &= \omega_{ce}^e \times \delta p^c + \delta v^c \\ \dot{\psi} &= -\omega_{ic}^c \times \psi - C_b^p \delta \omega_{ib}^b \end{aligned} \right\} \quad (4)$$

where $\delta\dot{v}^c$ and $\delta\dot{p}^c$ are velocity and position error vectors in c-frame, respectively; $\dot{\psi}$ is attitude error vector; f^c is the specific force in c-frame; C_b^P is the rotation matrix from the body coordinate system (B-frame) to the platform coordinate system (P-frame); ω_{ce}^e is angular velocity from c-frame to e-frame in e-frame; ω_{ic}^c is angular velocity from I-frame to c-frame in c-frame; ω_{ie}^c is angular velocity from I-frame to e-frame in c-frame; δf^b and $\delta\omega_{ib}^b$ are uncertainty of accelerometer and gyroscope,

respectively; Usually, δf^b and $\delta\omega_{ib}^b$ is modeled as scale factor error, bias error, and white noise:

$$\left. \begin{aligned} \delta f^b &= B_a + \text{diag}(f^b)S_a + \varepsilon_v \\ \delta\omega_{ib}^b &= B_g + \text{diag}(\omega_{ib}^b)S_g + \varepsilon_\varphi \end{aligned} \right\} \quad (5)$$

where B_a and B_g are the bias error of accelerometer and gyroscope, respectively; S_a and S_g are the scale factor error of accelerometer and gyroscope, respectively; ε_v and ε_φ are the processing noise error of velocity and angular rate, respectively; $diag()$ is the diagonal matrix;

The errors of accelerometer and gyroscope are modeled as first-order Gauss–Markov processes (Shin 2005):

$$\begin{cases} \dot{B}_a = \frac{-1}{\tau_{ba}} + \omega_{ba} \\ \dot{S}_a = \frac{-1}{\tau_{sa}} + \omega_{sa} \\ \dot{B}_g = \frac{-1}{\tau_{bg}} + \omega_{bg} \\ \dot{S}_g = \frac{-1}{\tau_{sg}} + \omega_{sg} \end{cases} \quad (6)$$

where ω and τ are white noise and correlation time coefficient, respectively;

The state vector of the INS model is:

$$X_{INS} = [\delta p_{INS}^n \quad \delta v_{INS}^n \quad \delta \Psi \quad \delta B_a \quad \delta B_g \quad \delta S_a \quad \delta S_g] \quad (7)$$

(4)-(6) can be expressed as:

$$\dot{X}_{ins} = H_{ins}X_{ins} + G_{ins}\omega_{ins} \quad (8)$$

2.3 GNSS/INS tight coupled

Generally, the IMU center position and the GNSS receiver Phase center are different with each other. So we need to correct the GNSS antenna phase center to the IMU center through the arm error vector l^b :

$$p_{ins}^n = p_{GNSS}^n + C_b^n l^b \quad (9)$$

The state equation of tightly-coupled model can be expressed as:

$$\left. \begin{aligned} Z_{TC} &= H_{TC}X_{TC} + \zeta_{TC}, \zeta_{TC} \sim N(0, \omega_k) \\ X_{TC,k} &= \Phi_{k-1,k}X_{TC,k-1} + \xi_{k-1}, \xi_{k-1} \sim N(0, Q_k) \end{aligned} \right\} \quad (10)$$

where Z_{TC} , H_{TC} , X_{TC} , ζ_{TC} are the observation vector, design coefficient matrix, state vector, and observation noise, respectively; $\Phi_{k-1,k}$, ξ_{k-1} are state transition matrix and process noise, respectively;

The vector \mathbf{X}_{TC} consists of X_{INS} and X_{GNSS} :

$$\left. \begin{aligned} X_{TC} &= [X_{INS} \quad X_{GNSS}] \\ X_{GNSS} &= [\delta t_r \quad \delta t_r \quad Ion \quad Trop \quad DCB \quad N] \\ X_{INS} &= [\delta p_{INS}^n \quad \delta v_{INS}^n \quad \delta \Psi \quad \delta B_a \quad \delta B_g \quad \delta S_a \quad \delta S_g] \end{aligned} \right\} (11)$$

where t_r is clock drift;

In the tightly-coupled model, the doppler frequency shift is increased and the clock drift parameter is introduced. So, the

observation vector Z_{TC} are pseudo range, carrier, Doppler frequency shift, and ionospheric delay.

$$\begin{aligned} Z_p &= P - \|p_r^e - p_s^e - C_n^e C_b^n l^b\| - \Delta P + \eta_p \\ Z_L &= L - \|p_r^e - p_s^e - C_n^e C_b^n l^b\| - \Delta L + \eta_L \\ Z_D &= D - \|v_r^e - v_s^e - [(\omega_{in}^n \times) C_b^n l_b + C_b^n (l_b \times) \omega_{ib}^b]\| - \Delta D + \eta_D \\ Z_{I_{GIM}} &= Ion \end{aligned} \quad (12)$$

where ΔP , ΔL and ΔD are the unmodeled errors in pseudo range, carrier, and doppler observations, respectively;

Designed coefficient matrix H_{TC} can be expressed as

$$H_{TC} = \left[\begin{array}{ccccccc} H_1 & 0 & H_2 & 0 & 0 & 0 & H_3 & 0 \\ H_1 & 0 & H_2 & 0 & 0 & 0 & H_3 & 0 \\ H_1 & 0 & H_2 & 0 & 0 & 0 & H_3 & 0 \\ H_1 & 0 & H_2 & 0 & 0 & 0 & H_3 & 0 \\ H_7 & H_8 & H_9 & 0 & H_{10} & 0 & H_{11} & 0 & H_{12} \\ H_7 & H_8 & H_9 & 0 & H_{10} & 0 & H_{11} & 0 & H_{12} \\ I & H_4 & H_1 & 0 & 0 & -I & & \\ I & H_4 & H_1 & 0 & 0 & -\gamma I & & \\ I & H_4 & 0 & I & 0 & I & & \\ \dots & & I & H_4 & 0 & 0 & I & \gamma I \\ 0 & 0 & 0 & 0 & 0 & 0 & & \\ 0 & 0 & 0 & 0 & 0 & 0 & & \end{array} \right] \quad (13)$$

where γ are the ionospheric conversion coefficient, $H_1 \sim H_{14}$ as follows:

$$\left. \begin{aligned} H_1 &= AC_1 \\ H_2 &= H_1(C_b^n l_b \times) \\ H_3 &= H_{12} = [1 \cdots 1]^T \\ H_4 &= [M_{wet,1} \cdots M_{wet,m}]^T \\ H_5 &= H_3 \beta \\ H_6 &= H_3 \alpha \\ H_7 &= AC_2 D^{-1} \\ H_8 &= AC_n^e \\ H_9 &= -H_8[(\omega_{en}^n \times + \omega_{ie}^n \times) C_b^n (l^b \times) + \\ &\quad + H_7(C_b^n l_b \times) \\ H_{10} &= -H_8 C_b^n (l^b \times) \\ H_{11} &= H_{10} \text{diag}(\omega_{ib}^b) \\ A &= (p_r^e - p_s^e - C_n^e C_b^n l^b) / \rho_{INS} \end{aligned} \right\} \quad (14)$$

The state transition matrix $\phi_{k-1,k}$ top 21×21 is consistent with H_{INS} . The state transition matrix receiver clock error and receiver clock drift is $\begin{bmatrix} 1 & \Delta t \\ 0 & 1 \end{bmatrix}$. The state transition matrix of other GNSS parameters are an identity matrix, and the parameters of GNSS and ins are independent of each other.

Fig. 1 is the structure of the GNSS/INS tightly-coupled navigation algorithm structure. The algorithm of the GNSS data processing part refers to the open-source code ‘GAMP’ (Zhou et al., 2018). The algorithm of the INS data processing part refers to AINS (Shin, 2005). Since the sampling rate of IMU data is much higher than that of GNSS data, INS completes the update of state vector separately when GNSS data is not updated. When GNSS data is updated, GNSS data and INS navigation results are filtered, and then new navigation results are output. The new deviation and scale factor of the gyro and accelerometer are used to compensate the IMU data of the next epoch.

3. EXPERIMENTAL RESULTS AND ANALYSIS

In order to analyze and verify the performance of GNSS/INS tightly-coupled algorithm, we collected two hours of dynamic data in Fozuling, Wuhan on July 20, 2018. The INS equipment is Lide A15. The corresponding parameters of the sensor and the parameters used in data processing in this paper are shown in Table 1. The sampling rate of IMU data is 200Hz. The GNSS receiver is Trimble R8, which can receive the observation data of GPS and BDS systems. The sampling rate is 1Hz. The GNSS data processing strategy is shown in Table 2. In addition, IGS final precise ephemeris product (sampling rate 900s) and precise clock error product (sampling rate 30s) are used for calculating satellite orbit and clock error respectively, and IGS DCB and GIM products are used for satellite DCB correction and calculating ionospheric delay respectively. The trajectory of this experiment is shown in Figure 2.

Table 1. IMU parameter

IMU parameter	
Angle random walk	0.003, deg/s/sqrt(h)
Velocity random walk	0.03, m/s/sqrt(h)
Gyro zero bias standard deviation	0.027, deg/h
Accelerometer zero deviation standard deviation	15, mGal
Gyro zero bias correlation time	4, h
Accelerometer zero bias correlation time	4, h
Lever arm compensation	[0.8, 0.65, -1.4](b frame)

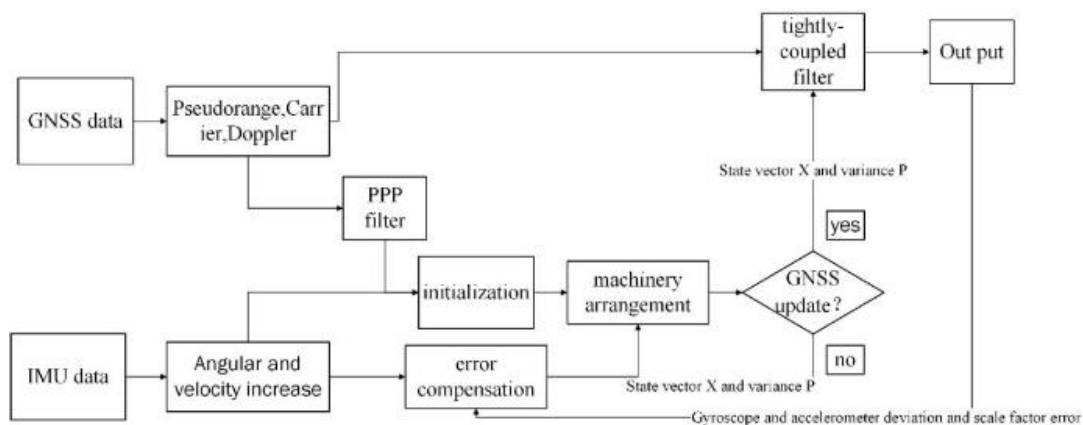


Figure 1. PPP/INS tightly-coupled navigation algorithm structure

3.2 Experimental result analysis

In order to analyze the performance of GNSS/INS tightly-coupled algorithm, the performance of GNSS and GNSS/INS tightly-coupled positioning is compared. Since the positioning result of GNSS/INS tightly-coupled is based on the center of inertial sensor, it is necessary to correct the positioning result of GNSS to the positioning result of integrated navigation, as shown in the following formula:

$$P_{INS}^e = P_{GNSS}^e - C_n^e C_b^n l^b \quad (15)$$

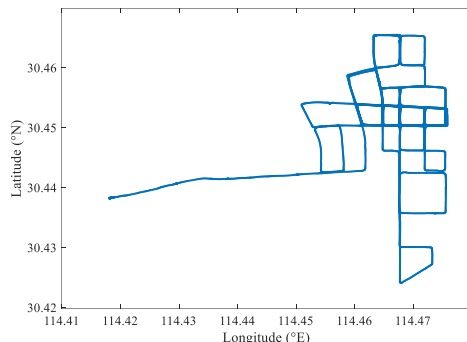


Figure 2. Trajectory

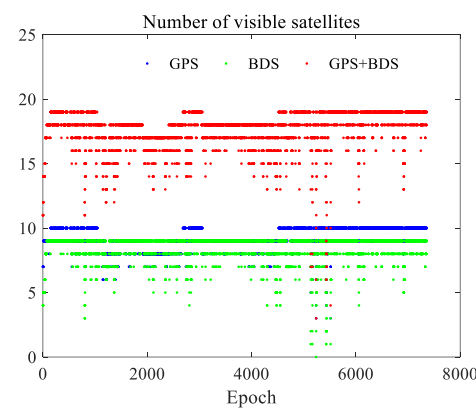
Table 2. GNSS data processing strategy

parameter	
Receiver clock error	White noise
Receiver clock drift	Random walk
Ionospheric delay	Random walk
Tropospheric wet delay	Random walk
Ambiguity	Random walk
Tropospheric dry delay、 PCO、PCV、Solid tide、 phase winding, etc	Empirical model correction

3.1 Experimental data analysis

Figure 3 counts the number of visible satellites and position dispersion of precision (PDOP) values of BDS and GPS systems. As shown in the figure, the number of GPS satellites observed is slightly more than that of BDS satellites, with an average of visible satellites are 8.54 and 9.25 respectively. The average observable satellites of the two systems are 17.8. The average PDOP value of GPS is 2.46 and the average PDOP value of GPS + BDS satellite is 1.35. It indicates that the spatial geometric distribution of the satellite has been significantly improved after adding BDS satellites. This shows that the field of vision of the experimental site is relatively wide and the observation conditions of GNSS are good. It is worth noting that GNSS data signal interruption occurred around LT 10:50, the number of observable satellites of GPS and BDS decreased significantly, and the PDOP value increased significantly.

Figure 4 shows the positioning error of GNSS and GNSS/INS tight combination in the end direction. Due to the weak satellite signal during 10:50, the positioning accuracy of two algorithms is affected. The GNSS is affected more seriously. It proves that when there are few or no GNSS observations, GNSS/INS integrated navigation can provide higher-precision and more stable positioning results. Table 3 counts the root mean square (RMS) values of the positioning errors of the two algorithms in the END (East, North, Down) direction, Horizontal and 3D. The horizontal positioning error difference between the two algorithms is very small, which are 0.86m and 0.71m respectively. However, in the D direction, the positioning error is 2.3 m and 0.9 m respectively. Compared with the GNSS, the tightly-coupled positioning accuracy has been significantly improved by 62.3% respectively. The 3D positioning accuracy of the two algorithms are 2.5 and 1.3 m respectively. Compared with GNSS positioning results, the tight combination positioning accuracy is improved by 54.9%.



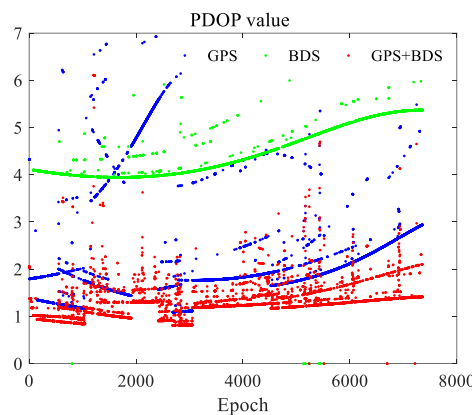


Figure 3. Number of visible satellites (up) and PDOP value (down)

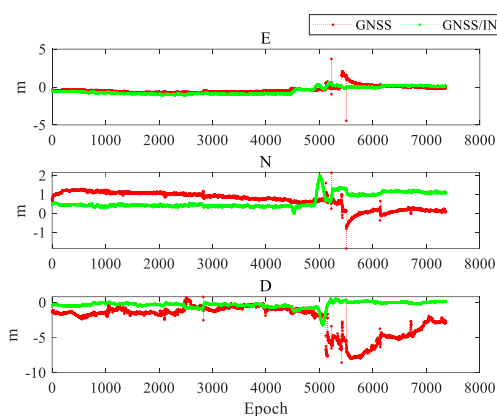


Figure 4. Position error of GNSS and GNSS/INS tightly-coupled in END direction

As shown in figure 5, the velocity error of GNSS/INS tightly-coupled are -0.02 to 0.02m/s in E and N direction, -0.05 to 0.05 in D direction. As table 4, the RMS of velocity error in END direction are 3.4, 3.5 and 4.1 mm/s respectively. Similarly, the velocity error also fluctuates slightly in the period of week GNSS signal. Figure 6 presents the attitude angle error of GNSS/INS tightly-coupled. The error of roll and pitch angle are small relative to heading angle. As table 5, the RMS of attitude angle (Roll, Pitch, Heading angle) error are 0.08, 0.05, 0.44' respectively. It is worth noting that the attitude angle is not affected in the period of week GNSS signal. This shows that the attitude angle is a little affected by the GNSS observation.

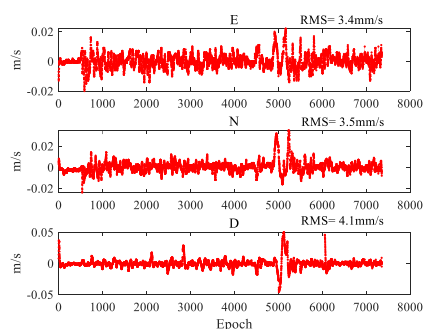


Figure 5. Velocity error of GNSS/INS tightly-coupled in END direction

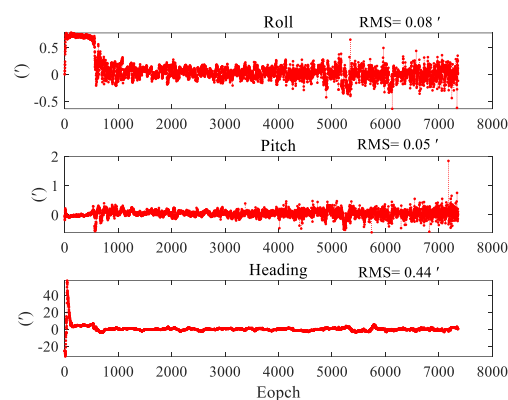


Figure 6. Attitude angle error of GNSS/INS tightly-coupled

Table 3. Position error in END direction

	GNSS RMS(m)	GNSS/INS RMS(m)	improve
E	0.47	0.45	-
N	0.72	0.55	14.2%
D	2.38	0.90	62.3%
Horizontal	0.86	0.71	17.4%
3D	2.53	1.14	54.9%

As shown in figure 7, the residual value of carrier observation (L1 and L2) is -1 to 1cm, and the RMS is 6mm and 8mm respectively. Relative to high-precision carrier observations, the residual value of pseudo range observation (P1 and P2) is -1 to 1 m, and the RMS is 0.56m and 0.51m respectively. The residual value of doppler (D1) is -0.5 to 0.5 m, and the RMS is 0.08m. The RMS values of the residuals of pseudo range, carrier and Doppler observations are within three times of their a priori accuracy, and the a priori accuracy is 0.3m, 0.003m and 0.1m respectively. This shows that the quality of GNSS observation data in this experiment is good.

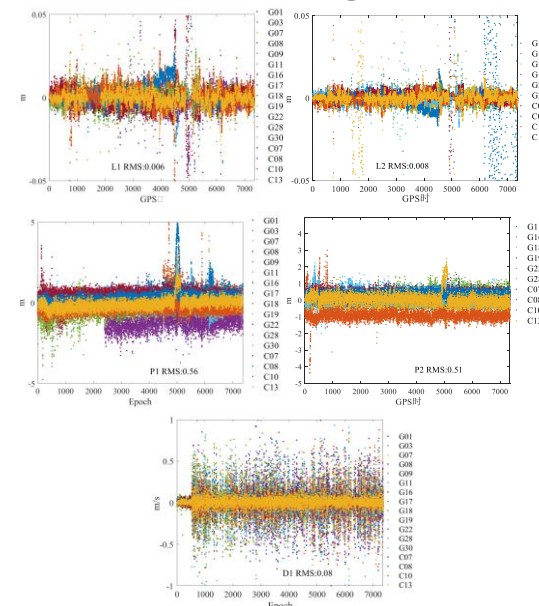


Figure 7. GNSS observation residual of GNSS/INS tightly coupled

4. CONCLUSION

In order to obtain a high-precision and robust kinematic vehicle navigation result under the urban environment, we design

GNSS/INS tightly-coupled navigation software for land vehicles. In order to verify the performance of the algorithm, we collected a set of on-board GNSS and INS data under the urban environment. The whole experiment lasted two hours around Fozuling, Wuhan.

The experimental results show that the E and N direction position precision is better than 0.5m and the D direction position precision is better than 1m. Compared to GNSS, the positioning precision of GNSS/INS tightly-coupled navigation in D direction and 3D improves 62.3% and 54.9 respectively. The velocity precision and attitude precision of GNSS/INS is very high, within 1mm/s and 1'. And The residual value of GNSS observation are lower than their triple priori variance, it proves that the quality of GNSS observation data in this experiment is good. The experimental results show that GNSS/INS tightly-coupled can provide higher precision and robust navigation and positioning results.

ACKNOWLEDGEMENTS

This work was supported in part by the Major Basic Research Project (5140503A0301), the National Natural Science Foundation of China (42174050), and the Provincial and Municipal "Double First-Class" Construction Project (600460035).

REFERENCES

- Abdolkarimi, Elahe Sadat, and Mohammad-Reza Mosavi 2020. A low-cost integrated MEMS-based INS/GPS vehicle navigation system with challenging conditions based on an optimized IT2FNN in occluded environments. *GPS Solutions* 24(4). <https://doi.org/10.1007/s10291-020-01023-9>
- Aykut, Nedim Onur 2018. The importance of meteorological variation on PPP positioning. *Measurement* 122:168-177. [10.1016/j.measurement.2018.03.027](https://doi.org/10.1016/j.measurement.2018.03.027)
- Chen, Kai, Guobin Chang, and Chao Chen 2021. GINav: a MATLAB-based software for the data processing and analysis of a GNSS/INS integrated navigation system. *GPS Solutions* 25(3). <https://doi.org/10.1007/s10291-021-01144-9>
- Erol, Serdar 2020. A Comparative Study for Performance Analysis of Kinematic Multi-Constellation GNSS PPP in Dynamic Environment. *Journal of Marine Science and Engineering* 8(7), 514.
- Falco, G., M. Pini, and G. Marucco 2017. Loose and Tight GNSS/INS Integrations: Comparison of Performance Assessed in Real Urban Scenarios. *Sensors (Basel)* 17(2).
- Gu, Shengfeng, et al. 2021. Multi-GNSS PPP/INS tightly coupled integration with atmospheric augmentation and its application in urban vehicle navigation. *Journal of Geodesy* 95(6).
- Guo, Jing, et al. 2018. Multi-GNSS precise point positioning for precision agriculture. *Precision Agriculture* 19(5):895-911.
- Guo, Wen, et al. 2019. Detection and Monitoring of Tunneling-Induced Riverbed Deformation Using GPS and BeiDou: A Case Study. *Applied Sciences* 9(13).
- Jiang, Chen, et al. 2021. Performance evaluation of the filters with adaptive factor and fading factor for GNSS/INS integrated systems. *GPS Solutions* 25(4).
- Kong, X., E. M. Nebot, and Hugh Durrant-Whyte 1999. Development of a nonlinear psi-angle model for large misalignment errors and its application in INS alignment and calibration. *IEEE International Conference on Robotics & Automation*, 1999.
- Li, Pan, et al. 2020. GPS + Galileo + BeiDou precise point positioning with triple-frequency ambiguity resolution. *GPS Solutions* 24(3).
- Li, Xin, et al. 2021. Improving PPP-RTK in urban environment by tightly coupled integration of GNSS and INS. *Journal of Geodesy* 95(12).
- Li, Z., et al. 2014. A Vondrak low pass filter for IMU sensor initial alignment on a disturbed base. *Sensors (Basel)* 14(12):23803-21.
- Shi, B., et al. 2021. Effect Analysis of GNSS/INS Processing Strategy for Sufficient Utilization of Urban Environment Observations. *Sensors (Basel)* 21(2).
- Shin E H. 2005. Estimation techniques for low-cost inertial navigation[D]. Doctoral dissertation, University of Calgary, Calgary, Canada,
- Zhang, Chuang, et al. 2020. Adaptive Fault Isolation and System Reconfiguration Method for GNSS/INS Integration. *IEEE Access* 8:17121-17133.
- Zhao, Hongwei, et al. 2020. A novel demodulation algorithm for VHF Data Broadcast signals in multi-sources augmentation navigation system. *International Journal of Distributed Sensor Networks* 16(3).
- Zhou, Feng, et al. 2018. GAMP: An open-source software of multi-GNSS precise point positioning using undifferenced and uncombined observations. *GPS Solutions* 22(2).